The Role of β Chains in the Control of the Hemoglobin Oxygen Binding Function: Chimeric Human/Mouse Proteins, Structure, and Function‡

Richard D. Kidd,§ J. Eric Russell,⊥ Nicholas J. Watmough,# Edward N. Baker,§ and Thomas Brittain*,§

School of Biological Sciences, Private Bag 92019, University of Auckland, Auckland, New Zealand, Department of Medicine, Children's Hospital of Philadelphia, University of Pennsylvania, Philadelphia, Pennsylvania 19104, and School of Biological Science, University of East Anglia, Norwich NR4 7TJ, U.K.

Received June 25, 2001

ABSTRACT: By using transgenic methodologies, we have produced a number of mouse/human chimeric hemoglobins containing adult mouse and human embryonic globin chains. A detailed analysis of the oxygen binding properties of these proteins identifies the dominant role played by the specific β-type globin chains in the control of the oxygen binding characteristics. Further analysis traces the origins of these effects to alterations in the properties of the T states of these proteins. The human ζ/mouse β chimeric protein has been crystallized, and its structure has been determined by X-ray diffraction to a resolution of 2.1 Å with R (R_{free}) values of 21.6% (24.9%). Close examination of the structure indicates that the subunit interfaces contain contacts which, although different from those present in either the parent human or the parent mouse proteins, retain the overall stabilizing interactions seen in other R state hemoglobins.

In recent years, much interest and experimental work has been directed toward the production of potential "blood substitutes" and the treatment of hemoglobin-related diseases, based on modifications of naturally occurring hemoglobin molecules (*1*−*4*). In one approach to blood substitutes, human adult hemoglobin has been transgenically expressed in a number of different species (*5*−*8*). However, in the case of expression in pigs, it has been found that expression of adult human α and β globins in the presence of pig globin synthesis, in vivo, does not lead to the production of all the chimeras possible by globin exchange (*9*). These data highlight potential problems of chain incompatibility not previously realized. Thus, a more detailed investigation of globin chain interactions is necessary before transgenic production of adult human hemoglobin is fully understood.

In the case of hemoglobin-related diseases, much research has been undertaken into the potential use of "unnatural" hemoglobins. Many hemoglobinopathies arise either from unbalanced synthesis of the constituent globin chains, for example, in the thalassemias, or from a mutant form of just one of the globin chains, for example, sickle cell disease (*10*). One potential route toward the treatment of such defects would be to induce the expression of a previously developmentally suppressed embryonic or fetal globin chain to replace the defective chain and produce within the circulation "developmental" chimeras which retain a functional adult globin in association with a fetal or embryonic partner globin chain (*11*). Indeed, fetal globin synthesis has been successfully achieved in adults on administration of hydroxyurea or butyrates (*12*−*19*). To examine further the potential of this approach, it is necessary to investigate the properties of such developmental chimeric proteins with regards both to their oxygen binding properties and to their subunit interactions.

All vertebrate hemoglobin proteins consist of quaternary structures containing two α- and two β-type globin protein subunits in which each subunit makes contacts with both similar and dissimilar chains. Within a given species, hemoglobins produced at different developmental stages often share a common globin chain while retaining allosteric function. Over the years, much data have been collected which indicate that within the hemoglobin molecule, the α and β globins are functionally nonequivalent, even though they are structurally very similar (*20*−*22*). It is thus important to establish how the globin chains interact with each other and how the functional properties of the heterotetramer are influenced by their constituent globin chains. To enable this, we have produced a number of transgenic mice that express adult mouse/embryonic human hemoglobin chimeras (*23*) which allows us to consider the oxygen binding properties of these proteins in detail. Moreover, we have obtained high-resolution structural data for one of these chimeras which allows us, for the first time, to investigate at the atomic level the interactions between the subunits of a chimeric hemoglobin protein.

MATERIALS AND METHODS

Assays. Chimeric hemoglobins were obtained from transgenic mice and purified as previously described (*24*−*26*).

‡ Crystal structure: The coordinates and structure factors for CO-$\zeta^{h}{}_{2}\beta^{m}{}_{2}$ have been deposited with the RCSB Protein Data Bank with accession numbers 1JEB and R1JEBSF, respectively.

* To whom correspondence should be addressed. Telephone: +64-9-373-7599 ext 8246. Fax: +64-9-373-7414. E-mail: T.Brittain@auckland.ac.nz.

§ University of Auckland.

⊥ University of Pennsylvania.

University of East Anglia.

[1] Abbreviations: Hb, hemoglobin; human, h; mouse, m; CO, carbon monoxide; $\zeta^{h}{}_{2}\beta^{m}{}_{2}$, chimeric human zeta2/mouse beta2 hemoglobin; $\alpha_2\beta_2$, human adult hemoglobin; MePEG, methoxypoly(ethylene glycol); rms, root-mean-square.

10.1021/bi011329f CCC: $20.00
Published on Web 11/22/2001

Oxygen binding curves were obtained on hemoglobin samples at approximately 100 μM protein concentration using an automated method employing a Hemox Analyzer (TCS, Hungtington Valley, PA) (*27*). Oxygen binding curves were analyzed in terms of the two-state model using in-house computer programs as previously described (*28*). Binding curves were obtained at 37 °C in 20 mM HEPES buffer containing 1 mM EDTA and 100 mM NaCl at pH 7.4.

Oxygen dissociation rates were determined using anaerobic stopped-flow mixing of the oxygenated proteins with an excess of sodium dithionite using a modified Applied Photophysics Ltd (Leatherhead, Surrey, U.K.) DX17MV stopped-flow spectrophotometer. The kinetics of oxygen binding to the R state of the hemoglobins were determined by following the time course of oxygen reassociation with the transiently partially (approximately 5%) deoxygenated form of the proteins produced by partial photolysis using the signal from the second harmonic output (10 ns, 100 mJ) of a SL282G Nd:YAG laser (Spectron, Rugby, Warks, U.K.) interfaced to an Applied Photophysics Ltd LKS.50 laser flash photolysis spectrometer (*28*). Time courses for the kinetic reactions were followed at 436 nm in 20 mM HEPES buffer containing 1 mM EDTA and 100 mM NaCl at pH 7.4 and 37 °C. Reaction curves for the time course of deoxygenation and oxygen association were analyzed in terms of the sum of two exponential processes employing proprietary software (*Tablecurve-2D,* Jandel Scientific, San Rafael, CA).

Crystallization and Data Collection. The $\zeta_2\beta_2$ crystals used in this work were of the carbonmonoxy form. To stabilize the protein and prevent oxidation, the protein was saturated with carbon monoxide, and 2 mM sodium dithionite was added prior to crystallization. Crystallization conditions were found by a sparse matrix search procedure (*29*). Crystals were grown by hanging-drop vapor diffusion at 18 °C in 2 μL drops by mixing equal volumes of the protein solution (30 mg/mL in 0.1 M HEPES buffer (pH 7.4) with 2 mM sodium dithionite) with reservoir solution. Crystallization trays were stored in the dark. The best-diffracting crystals (0.4 × 0.4 × 0.4 mm) grew in a drop equilibrated over a reservoir solution of 0.1 M Bicine/NaOH (pH 8.5) and 33% MePEG 550.

The crystals were tetragonal, $P4_1$, with unit-cell parameters $a = b = 84$ Å and $c = 104$ Å with one heterotetramer in the asymmetric unit. The crystal density (V_m) is calculated to be 2.92 Å^3 Da^{-1} with a solvent content of 58% (v/v) (*30*). An initial data set was collected in-house to a resolution of 2.5 Å using a single flash-frozen crystal. X-ray data were collected at 110 K using a MAR Research 345 image plate detector with Cu Kα radiation from a Rigaku RU-H3R rotating anode generator equipped with focusing mirrors. Data were collected as a series of 1° oscillation frames, each of 15 min exposure, at a crystal to detector distance of 235 mm. A second data set was collected on another crystal with synchrotron radiation from beamline 9-2 ($\lambda = 1.00$ Å) at the Stanford Synchrotron Radiation Laboratory. This X-ray data set was collected at 110 K using an ADSC Quantum-4 (2 × 2) CCD detector to a resolution of 2.1 Å. Data were collected as a series of 1° oscillation frames, each of 10 s exposure, at a crystal to detector distance of 152 mm. Image data for both crystals were processed and scaled using the *DENZO* and *SCALEPACK* (*31*) software. Data collection statistics for both crystals are summarized in Table 1.

Table 1: Crystal and Data Collection Statistics

	crystal 1	crystal 2
source	RU-H3R	SSRL
space group	$P4_1$	$P4_1$
cell dimensions (Å):		
$a = b$	84.74	84.92
c	104.21	104.52
reflections measured	542 690	192 738
unique reflections	25 563	43 348
maximum resolution (Å)	2.5	2.1
completeness[a](%)	99.9 (100.0)	99.9 (100.0)
multiplicity[a]	21.2 (13.8)	4.4 (3.9)
R_{merge}[a,b] (%)	8.1 (62.7)	5.3 (46.5)
mean[a]$I/\sigma I$	10.7 (4.6)	11.5 (2.9)

[a] Figures in parentheses are for the outermost resolution shell: 2.59−2.50 Å for crystal 1 and 2.18−2.10 Å for crystal 2. [b] $R_{merge} = \sum_h\sum_i|I_{h,i}| - \langle I_h\rangle/\sum_h\sum_i|I_{h,i}|$

Table 2: Refinement and Model Statistics

resolution range (Å)	28.0−2.1
total number of reflections in range	43 240
R_{cryst} (%)	21.6
R_{free}[a] (%)	24.9
bond length rms deviation (Å)	0.007
bond angle rms deviation (deg)	1.2
Ramachandran plot:[b]	
residues in most favored region (%)	91.1
residues in disallowed region (%)	0.2
average B factor (Å^2):	
main chain-total	45.4
main chain-ζ1, ζ2, β1, β2	42.2, 40.2, 59.9, 39.2
side-chain-total	46.4
side-chain-ζ1, ζ2, β1, β2	43.7, 41.4, 60.2, 40.9
solvent	48.1
number of protein atoms	4371
number of heme atoms	172 (4 × 43)
number of ligand atoms	8 (4 C−O)
number of acetyl atoms (non-hydrogen)	6 (2 O=C−CH_3)
number of water molecules	234

[a] 10% randomly omitted reflections were used for R_{free}. [b] As defined by *PROCHECK* (*38*).

Structure Determination. The 2.5 Å data set was used to obtain an initial structure by molecular replacement. The search model was constructed from human adult ($\alpha_2\beta_2$) carbonmonoxy hemoglobin (PDB code 1BBB; (*32*)), in which side-chains that differed between human α and human ζ, and between human β and mouse β, were truncated to Ala or Gly. Using *CNS* (*33*), rotation and translation function calculations based on data between 15 and 4 Å gave a single unambiguous solution. After rigid-body refinement in which each subunit was treated as a separate rigid body, the R factor was 42.3% and R_{free} was 41.7%. For the R_{free} calculation (*34*) in this and subsequent refinement steps, 10% of the reflections were randomly selected. The model was then built into $2F_o - F_c$ and $F_o - F_c$ electron density maps using *O* (*35*). After a single round of simulated annealing using *CNS*, the missing side-chains for human ζ (ζ^h) and mouse β-Single (β^m) were built into the model. Mouse β-Single differs from mouse β-Major at three residues: Ala13 → Gly, Val20 → Ala, and Asn139 → Ala (*36*).

The 2.5 Å model was then used as a starting model for refinement against the 2.1 Å data. The structure was refined by alternating cycles of *CNS* refinement (using data between 25 and 2.1 Å) with model rebuilding using *O*. Typically, *CNS* refinement included the following steps (in order): simulated annealing, individual B-factor refinement, water

Table 3: Comparison of Oxygen Binding Characteristic of Human and Mouse Adult, Human Embryonic, and Human/Mouse Chimeric Hemoglobins[a]

protein	p_{50}	n	Bohr	K_T	K_R	L	k_{off}	k_{on}
$\alpha^m\beta^m$	17	2.5	−0.60	42	0.4	1.5×10^6	54, 125	3.9×10^7, 1.3×10^8
$\zeta^h\beta^m$	14	2.4	−0.17	42	0.8	2.5×10^5	16, 160	2.0×10^7, 1.5×10^8
$\alpha^h\beta^m$	21	2.9	−0.52	56	0.9	4.0×10^5	25, 139	4.5×10^7, 1.5×10^8
$\alpha^h\beta^h$	9	2.9	−0.41	21	0.3	5.0×10^5	12, 40	4.2×10^7, 1.4×10^8
$\alpha^m\beta^h$	8	2.2	−0.84	22	0.7	1.2×10^4	58, 58	3.8×10^7, 2.0×10^8
$\alpha^m\epsilon^h$	6	2.2	−0.62	15	0.9	1.1×10^3	63, 62	7.5×10^7, 7.5×10^7
$\zeta^h\epsilon^h$	4	2.3	−0.30	12	0.5	1.8×10^3	11, 60	2.4×10^7, 9.0×10^7
$\zeta^h\gamma^h$	6	2.3	−0.30	8	0.3	6.0×10^4	11, 70	4.0×10^7, 9.0×10^7

[a] m refers to mouse, and h refers to human. p_{50} values are in mmHg partial pressure of oxygen. n is the Hill coefficient. Bohr is the slope of the plot of log(p_{50}) versus pH. K_T and K_R are, respectively, the equilibrium constants for the reaction of oxygen with the T and R states. L is the allosteric equilibrium constant. k_{off} represents the oxygen dissociation rate constants for the α and β chains, respectively, in units s^{-1}. k_{on} represents the oxygen association rate constants for the α and β chains, respectively, in units of M^{-1} s^{-1}.

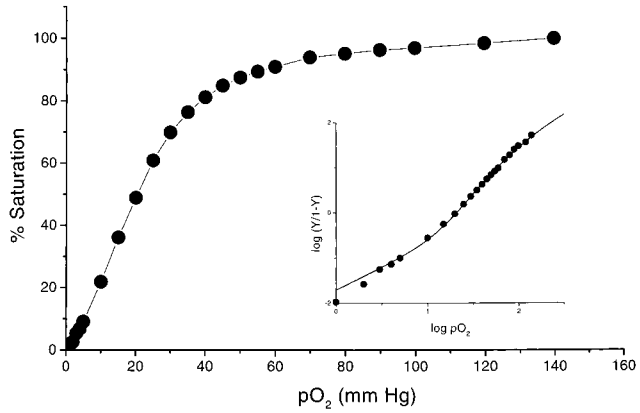

FIGURE 1: Oxygen binding curve for $\zeta^h{}_2\beta^m{}_2$ chimeric hemoglobin. The experimental oxygen binding data (•) for a sample of 100 μM $\zeta^h{}_2\beta^m{}_2$ hemoglobin are shown as compared to the best fit two state allosteric model (—), obtained using the parameter set detailed in Table 3. Data were recorded at pH 7.4 in 20 mM HEPES buffer containing 100 mM NaCl at 37 °C. Inset is a Hill plot of the data.

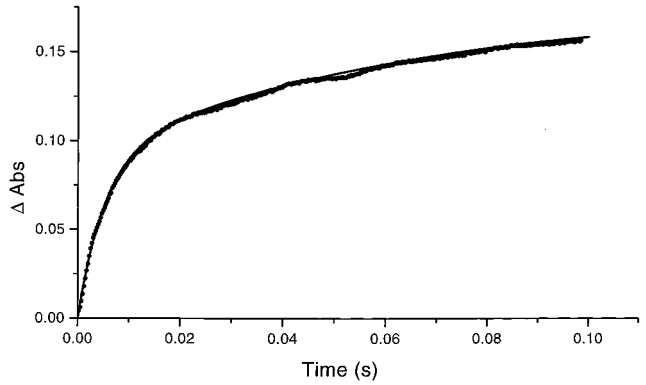

FIGURE 2: Oxygen dissociation from $\zeta^h{}_2\beta^m{}_2$ chimeric hemoglobin. The time course for oxygen dissociation from chimeric $\zeta^h{}_2\beta^m{}_2$ hemoglobin (•) is shown as compared to the best fit double exponential model (—). The reaction was performed in 20 mM HEPES buffer, containing 100 mM NaCl, at pH 7.4 and 37 °C. The progress of the reaction was monitored at 436 nm.

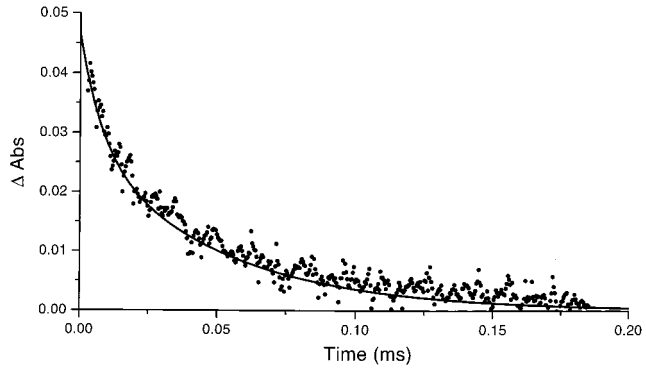

FIGURE 3: Oxygen reassociation with $\zeta^h{}_2\beta^m{}_2$ chimeric hemoglobin. The time course for the recombination of chimeric $\zeta^h{}_2\beta^m{}_2$ hemoglobin with 1.1 mM oxygen following 2% partial photodissociation (•) is shown compared with the best fit double exponential model (—). The reaction was monitored at 436 nm in 20 mM HEPES buffer, containing 100 mM NaCl, at pH 7.4 and 37 °C, following a 6 ns laser photolytic pulse.

picking, and conjugate gradient minimization refinement. This resulted in minimal change. The final R (R_{free}) values were 21.6% (24.9%). Full refinement statistics are given in Table 2. Structural superpositions were carried out with the program *LSQKAB* from the CCP4 program suite (*37*), and the quality of the final model was analyzed with *PROCHECK* (*38*).

RESULTS

Functional Studies. The nomenclature for describing the various globins in this study is as follows: human alpha, beta, zeta, gamma, and epsilon chains are labeled α^h, β^h, ζ^h, γ^h, and ϵ^h, respectively; mouse beta is β^m. The chimeric proteins exhibit moderate oxygen binding constants and normal degrees of cooperativity at 37 °C (Table 3), consistent with the values for these proteins previously determined at a lower temperature (*39*). The oxygen affinities of the proteins appear to fall into two distinct subgroups: 6−8 mmHg and 21−29 mmHg. Detailed analysis of the oxygen binding curves using the two-state model (Figure 1) shows β^m-containing molecules have significantly lower T state affinity for oxygen than β^h- or ϵ^h-containing proteins. The R state equilibrium constant for oxygen binding, however, is essentially independent of the particular structure. The Bohr coefficient shows no obvious correlation with the type of chains present in the particular hemoglobin molecules. The allosteric constants (L) associated with all the β-containing chimeric proteins are moderately high, while the $\alpha^m{}_2\epsilon^h{}_2$ protein shows a significantly lower L value. Oxygen dissociation kinetics (Figure 2) indicate chain equivalence in α^m-containing proteins but significant chain kinetic heterogeneity in the β^m-containing proteins. Oxygen association rate measurements (Figure 3) show chain equivalence in the R state of $\alpha^m{}_2\epsilon^h{}_2$ but chain heterogeneity in the other hemoglobin molecules.

Quality of the $\zeta_2\beta_2$ Structural Model. The crystal structure of CO-$\zeta^h{}_2\beta^m{}_2$ contains a single $\zeta_2\beta_2$ heterotetramer in the asymmetric unit. Refinement at 2.1 Å resolution has given excellent agreement with the X-ray data, with a final crystallographic *R* factor of 21.6%, a free *R* factor of 24.9%, and a model that conforms very well with standard protein geometry. Root-mean-square (rms) deviations from standard bond lengths and angles are 0.007 Å and 1.2°, respectively (Table 1), and 91.1% of the residues are in the most favored region of the Ramachandran plot, as defined by *PROCHECK* (*38*). Only one residue, β^m2 145Tyr, is in a disallowed region.

The final model comprises residues 1−141 for both ζ^h chains, residues 1−143 for the β^m1 chain, and residues 1−146 for the β^m2 chain. In general, the electron density describing the model is of high quality, except for a few side-chains and the C-terminal residues of ζ^h2, β^m1, and β^m2. No density was visible even to low σ levels for the three terminal residues of β^m1; these residues are thus not included in the model. The model also includes four hemes, four CO molecules, two acetyl groups, which are present on the N-termini of both ζ^h chains, and 234 water molecules. The electron density is not as clear for the CO of β^m1 as compared to the other three chains' CO molecules.

Interestingly, the average *B* factors for β^m1 are approximately 20 Å^2 higher than for the other three chains (average main-chain *B* factors for ζ^h1, ζ^h2, β^m1, and β^m2 are 42.2, 40.2, 59.9, and 39.2 Å^2, respectively). Although large differences in average *B* factors between α- and β-type globins have been seen before in hemoglobin (*40*), it is unusual for just one chain to display such a marked difference. To further understand this result, intermolecular contacts were analyzed with the CCP4 program *DISTANG* (*37*): ζ^h1, ζ^h2, and β^m2 make 9, 10, and 12 intermolecular crystal contacts with symmetry-related molecules; β^m1 only makes a single contact. This lack of anchoring interactions probably contributes to the higher mobility (*B* factors) of β^m2. Other areas of concern regarding *B* factors are their high values (>40 Å^2, please see Table 2) and the small gap (∼1.5 Å^2) between main-chain and side-chain values. However, both of these results, although rare for hemoglobin structures, are not unprecedented; for example, similar results have been seen for human embryonic (*41*) and sea lamprey (*42*) hemoglobins. Perhaps it is not really appropriate to compare the *B* factors of the CO-$\zeta^h{}_2\beta^m{}_2$ structure to other hemoglobins; this is the first time that the human ζ chain and any mouse globin has been solved and the crystals were crystallized in a new space group ($P4_1$) with unique unit cell dimensions (Table 1) using a new (for hemoglobin) crystallization condition (MePEG 550). Mean *B* factors and full refinement details are in Table 2.

Molecular Structure. As a chimeric molecule, the $\zeta_2\beta_2$ protein comprises chains that are not usually paired in hemoglobins. Nevertheless, its overall quaternary structure conforms closely to that of other liganded hemoglobin molecules; the structure lies between the R and R2 state, though closer in orientation to the R state. When one $\zeta\beta$ dimer is superimposed on the R state $\alpha\beta$ dimer (*43*), it requires a further rotation of about 3° to superimpose the other halves of the two tetramers.

The mouse β chain has a structure that corresponds very closely to that of the human adult β chain (Figure 4A) and other β-type chains, diverging only at the N- and C-termini.

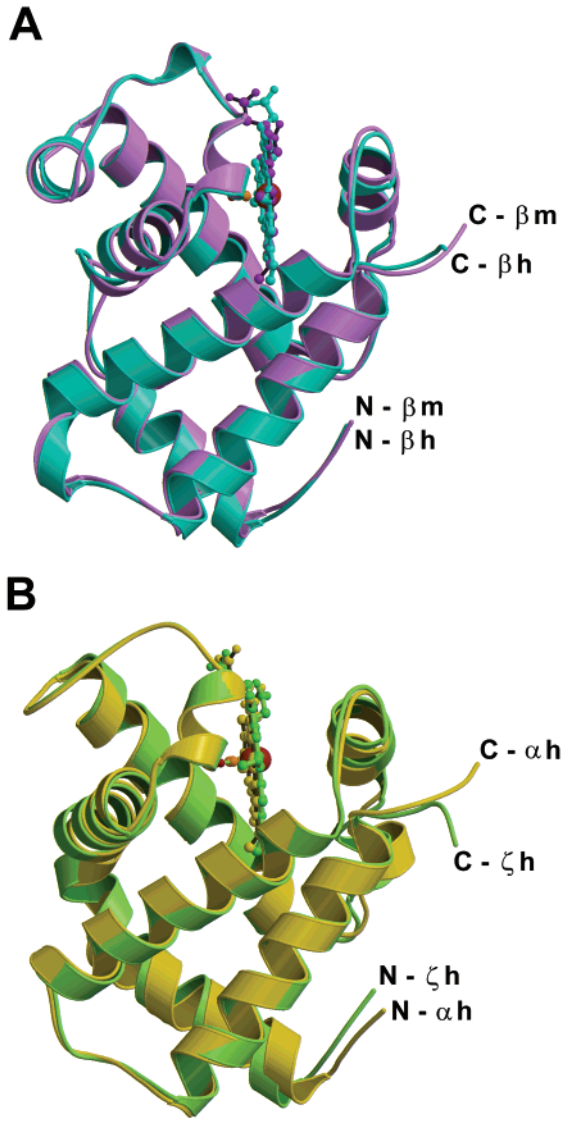

FIGURE 4: Superposition of human adult globins upon the globins of the CO-$\zeta^h{}_2\beta^m{}_2$ chimeric hemoglobin. The human adult globins are from CO-$\alpha_2\beta_2$, PDB entry 1BBB (*32*). (A) Ribbon diagram of human β (blue) superimposed onto mouse β (purple). (B) Ribbon diagram of human α (yellow) superimposed onto human ζ (green). Figures were drawn using the program *MOLSCRIPT* (*52*) and rendered with *RASTER3D* (*53*).

When residues 4−143 of the mouse β chain are superimposed on the equivalent residues of the human β chain (from CO-$\alpha_2\beta_2$, PDB entry 1BBB (*32*)), the rms difference, over all α carbon positions, is 0.63 Å, demonstrating the close alignment of these two β structures (81% sequence identity). This rms value is similar to those obtained in comparisons between the various liganded human β-type chains: 0.83 Å for human β−human γ (γ from CO-γ_4, PDB entry 1I3D (*44*)) and 0.62 Å for human β−human ε (ε from CO-$\alpha_2\epsilon_2$, PDB entry 1A9W (*41*)). The greater deviation between human β and human γ arises from a slight shift in the A helix of the γ chain relative to the β chain (*44*).

On the other hand, a comparison of the human embryonic ζ chain with that of the human adult α chain shows a number of significant differences. The N-termini of the ζ chains are clearly acetylated (Figure 5). The rms difference in α carbon positions between the ζ and α chains is 0.82 Å for residues 4−141 (i.e., omitting the three N- and C-terminal residues).

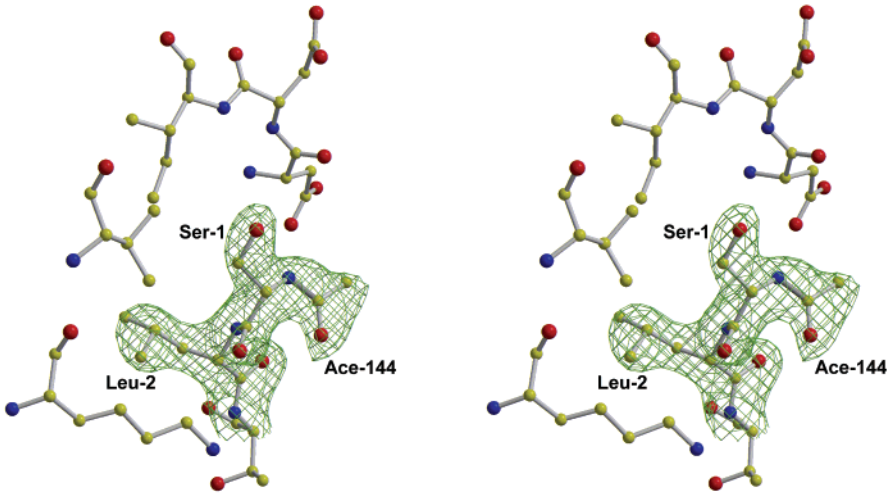

FIGURE 5: Stereoview of the N-acetylation site of one of the ζ chains (ζ^h2). The map was calculated with Fourier coefficients $2F_o - F_c$ and was contoured at 1.2σ. The N-terminal serine is N-acetylated in both ζ chains (ζ^h1 not shown). The figure was drawn using *BOBSCRIPT* (*54*) and *RASTER3D* (*53*).

The C-terminal C^α atoms have diverged by ~9 Å (Figure 4B); however, it must be remembered that the salt bridges at the C-termini in the T state are broken upon ligand binding, and this allows the termini to move freely in solution (*20*). The human ζ chain is the most divergent of the human hemoglobin subunits; the sequence identity between ζ and α is 60%.

Comparisons of the heme pockets between α^h and ζ^h and between β^h and β^m reveal no large surprises. However, in the ζ chains, Lys61 appears to form a weak ionic interaction with the heme propionate group. For $\zeta1$, the distance between the Lys61 N^ζ and the heme carbonyl O1A atom is 2.80 Å, while for $\zeta2$, the distance is 3.08 Å. Lys61 (Lys66 in β-like chains) is strictly conserved among the human hemoglobins. This interaction between the lysine side-chain and the propionate group has also been observed in structures containing the embryonic ϵ (*41*) and fetal γ (*45*) chains. This interaction in ζ, ϵ, and γ chains helps explain the higher heme affinities found in their respective embryonic methemoglobins relative to the adult methemoglobin (*46*).

DISCUSSION

Under physiological conditions, the mouse/human chimeric hemoglobins all exhibit oxygen binding characteristics which fall within the range observed in the adult mouse and adult human hemoglobins and the human embryonic hemoglobins (Table 3). Interestingly, exchange of subunits within these hemoglobins does not lead to a significant loss of cooperativity. The oxygen binding affinity of the chimeras on the other hand falls into two clear groups: a low affinity group containing β^m chains and a high affinity group containing β^h or ϵ^h chains. Similar characteristics have been reported previously in the cases of adult mouse/adult human (*47*), adult mouse/adult donkey (*48*), and adult human/adult pig (*9*) systems. The Bohr effect does not show any simple pattern as would be expected as this property of pH sensitivity is well recognized as containing contributions from both the α- and β-type chains. More detailed analysis of the oxygen binding curves in terms of the two-state model of cooperativity is also enlightening. The derived allosteric constant (L) has a higher value in the case of the β^m-containing hemoglobins than in the case of the β^h- or ϵ^h-containing hemoglobins, indicative of a more stable T state. In addition to the relative position of the allosteric equilibrium, we find that the T state forms of the β^m-containing chimeras also possess intrinsically lower oxygen affinity (K_T) than those of the β^h and ϵ^h cases, while exhibiting essentially identical R state affinities (K_R). A kinetic analysis of the oxygen dissociation rates indicates that in the R state, the β^m chains show a higher dissociation rate than the β^h or ϵ^h chain. This is accompanied in general by a somewhat higher association rate. Interestingly, if the R state equilibrium constants are calculated from the k_{off}/k_{on} values, then the differences in the kinetic rate constants are essentially self-compensating. The equilibrium constants for all the chains within the R state exhibit kinetically derived equilibrium constants in the range 0.2−0.8 mmHg, in good agreement with the equilibrium measurements.

Oxygen affinity and cooperativity are affected by heme pocket structure and subunit interface interactions. Since therapies for various hemoglobinopathies have been proposed using developmental chimeras, we determined the structure of a human embryonic/mouse adult chimera ($\zeta^h{}_2\beta^m{}_2$) to determine whether the combination of chains that are not normally paired would affect either the heme environment or the quaternary structure of the heterotetramer. In the absence of a structure for adult mouse hemoglobin, our structural comparisons had to be made via the human adult hemoglobin structure. Nevertheless, some interesting observations can be made. A comparison of the heme pockets of the α^h and ζ^h chains and the β^h and β^m chains shows no major structural variations. On the other hand, the subunit interfaces contain a number of amino acid substitutions. Within the $\zeta1\beta1$ interface, six amino acid differences are found when this interface is compared to the known human $\alpha1\beta1$ interface, as a result of substitutions in either the ζ chain (two residues) or the β^m chain (four residues). Some of these substitutions are shown in Figure 6. This interface contains a large number of weak to moderate interactions; 32 such interactions have been identified (*49*). The sum of these interactions is such that in adult human hemoglobin,

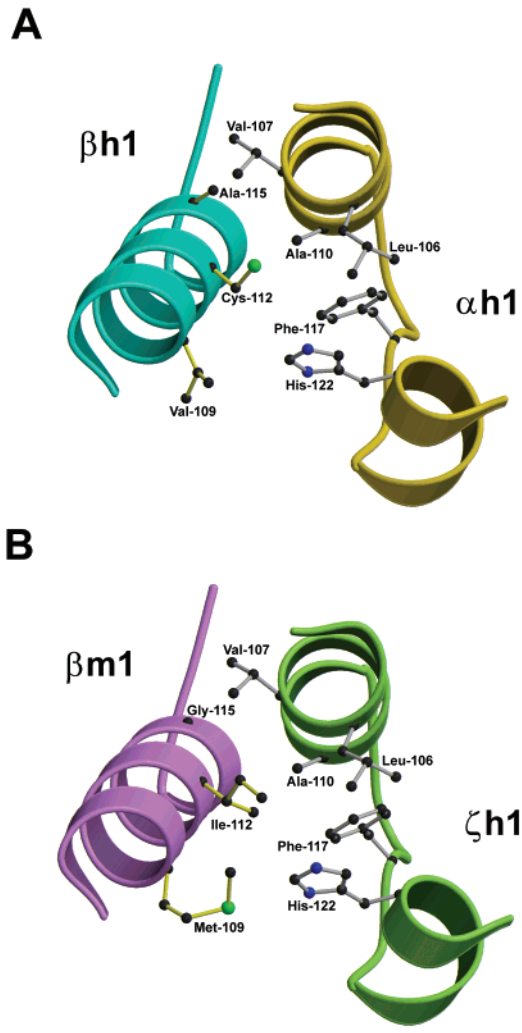

FIGURE 6: View of some of the residues at the $\alpha1\beta1$ interface for (A) human adult CO-$\alpha_2\beta_2$ and for (B) CO-$\zeta^h{}_2\beta^m{}_2$ chimeric hemoglobin. Although all but two of the α and ζ residues are conserved at this interface, there are a number substitutions between human and mouse β globins. The altered interactions are listed in Table 4. Figures were drawn using the program *MOLSCRIPT* (*52*) and rendered with *RASTER3D* (*53*).

the $\alpha1\beta1$ interface is considerably stronger than the corresponding $\alpha1\beta2$ interface and is only disrupted under extreme conditions. A detailed study of the $\zeta^h1\beta^m1$ interface indicates that although the amino acid differences between the α^h and ζ^h chains and the β^h and β^m chains lead to some altered interactions, these alterations are essentially compensatory (Table 4).

In contrast to the $\alpha1\beta1$ interface, the $\alpha1\beta2$ interface of the hemoglobin molecule is relatively weak, and the T to R transition, which occurs during oxygen binding, involves a significant shift in the relative positions of the $\alpha1\beta1$ and $\alpha2\beta2$ dimers. In the R state (oxygenated), the $\alpha1\beta2$ interface involves a few relatively strong amino acid interactions. In the case of the $\zeta^h{}_2\beta^m{}_2$ structure, the only alterations in the $\alpha1\beta2$ contact region arise from the single difference in the ζ^h chain as compared to the α chain at this interface. This difference consists of a $\alpha^h38\text{Thr} \rightarrow \zeta^h38\text{Gln}$ substitution. In the human adult protein, the Thr amino acid makes contacts with βHis97 and βAsp99 (these contacts are not present in the R2 state (*32*); the αThe38 has moved too far away). Close examination of the structure of the $\zeta^h{}_2\beta^m{}_2$ protein shows that

Table 4: Comparison of $\alpha^h1\beta^h1$ and $\zeta^h1\beta^m1$ Interface Interactions

amino acid 1[a]	amino acid 2[b]	interaction	present/absent
β^hVal109	αHis122	hydrophobic	
β^mMet109			+
β^hCys112	αLeu106	hydrophobic/polar	
β^mIle112			+
β^hCys112	αAla110	hydrophobic/polar	
β^mIle112			+
β^hCys112	αHis122	acid/base	−
β^mIle112	αPhe117	hydrophobic	+
β^hAla115	αVal107	hydrophobic	
β^mGly115			−
β^hPro125	αLeu34	hydrophobic	
β^mAla125			+
β^mPro124	αLeu34	hydrophobic	+
α^hHis112	βLys120	acid/base	
ζ^hArg112			+
α^hPro119	βMet55	hydrophobic	
ζ^hAla119			+

[a] Upper residue in $\alpha^h{}_2\beta^h{}_2$; lower residue in $\zeta^h{}_2\beta^m{}_2$. [b] Interacting amino acid in $\alpha^h{}_2\beta^h{}_2$.

the human αThr38 interaction with βHis97, which normally involves a hydrogen bond through solvent (αThr38 $O^{\gamma1}$−H_2O−βHis97 O), has been eliminated in the chimeric protein. However, the interaction between αThr38 and βAsp99 in the human protein has been replaced by two ζGln38−βAsp99 interactions in the human/mouse chimeric protein: ζGln38 $N^{\epsilon2}$−βAsp99 $O^{\delta1}$ and ζGln38 $O^{\epsilon1}$−βAsp99 $O^{\delta1}$ at 2.81 and 3.3 Å, respectively. In terms of the number of interactions across the $\zeta^h1\beta^m2$ interface, within the R state, the chimeric protein thus closely mirrors the situation present in the human protein. However, the chimeric protein does show a higher oxygen affinity and slightly lower cooperativity than the natural parent molecule. This same pattern of change has been observed in the adult human protein in which αThr38 is mutated to αGln38 (*28*). In this report, the change in reactivity was ascribed to the interaction involving αGln38 which stabilizes the T state (deoxy) structure. As well as chain−chain interactions, this mutation may also affect cooperativity via a purely steric effect on the T to R transition which involves the "ratcheting" of βHis97 from between αPro44 and αThr41 in the T state to between αThr41 and αThr38 in the R state.

Our structural studies clearly show that the N-terminus of the ζ chain is acetylated in $\zeta^h{}_2\beta^m{}_2$ molecules synthesized in the definitive red blood cells of the transgenic mice (Figure 5). The ζ chain is normally fully acetylated in embryonic hemoglobins synthesized in the yolk sac (*50*), while the γ chains of fetal hemoglobin are only partially acetylated in definitive red blood cells (*51*). Synthesis of ζ chains in definitive red blood cells thus does not lead to deacetylation, and the presence of acetylated ζ chains indicates that this modification is intrinsic to the amino acid sequence of the ζ chain and is not dependent on the nature of the red blood cells in which the synthesis occurs.

In conclusion, the combination of our structural and functional studies on chimeric hemoglobins synthesized in transgenic mice shows that significant compatibility exists between α- and β-type globin chains obtained from disparate origins. Furthermore, it is apparent that within these molecules, much of the reactivity with oxygen is governed by the nature of the β chain. These results clearly indicate the potential for the use of chimeric hemoglobins, either trans-

genic or developmental, in the relief of various hemoglobinopathies.

ACKNOWLEDGMENT

We thank Clyde Smith, Peter Haebel, and staff of the Stanford Synchrotron Radiation Laboratory for help with data collection.

REFERENCES

1. Looker, D., Abbott-Brown, D., Cozart, P., Durfee, S., Hoffmann, S., Mathews, A. J., Miller-Roehrich, J., Shoemaker, S., Trimble, S., Fermi, G., Komiyama, N., Nagai, K., and Stetler, G. L. (1992) *Nature 356*, 258−260.
2. Dracker, R. A. (1995) *Immunol. Invest. 24*, 403−410.
3. Waschke, K. F. (1995) *Anaesthesist 44*, 1−12.
4. Winslow, R. M. (1995) *Nature Med. 1*, 1212−1215.
5. Behringer, R. R., Ryan, T. M., Reilly, M. P., Asakura, T., Palmiter, R. D., Brinster, R. L, and Townes, T. M. (1989) *Science 245*, 971−973.
6. Greaves, D. R., Fraser, P., Vidal, M. A., Hedgs, M. J., Ropers, D., Luzzatto, L., and Grosveld, F. (1990) *Nature 343*, 183−185.
7. Swanson, M. E., Martin, M. J., O'Donnell, K., Lago, W., Huntress, V., Parsons, C. T., Pinkert, C. A., Pilder, S., and Logan, J. S. (1992) *Bio/Technology 10*, 557−559.
8. O'Donnell, K., Martin, M. J., Logan, J. S., and Kumar, R. (1993) *Cancer Detect. Prev. 17*, 307−312.
9. Rao, M. J., Manjula, B. N., Kumar, R., and Acharya, A. S. (1996) *Protein Sci. 5*, 956−965.
10. Loukoloulos, D. (1997) *J. Intern. Med. Suppl. 740*, 43−48.
11. Cappellini, N., and Beuzard, Y. (1998) *Hemoglobin 22*, 5−6.
12. Perrine, S. P., Faller, D. V., Swerdlow, P., Miller, B. A., Bank, A., Sytkowski, A. J., Reczek, J., Rudolph, A. M., and Kan, Y. W. (1990) *Ann. N. Y. Acad. Sci. 612*, 134−140.
13. Stamatoyannopoulos, J. A., and Nienhuis, A. W. (1992) *Annu. Rev. Med. 43*, 497−521.
14. Perrine, S. P., Olivieri, N. F., Faller, D. V., Vichinsky, E. P., Dover, G. J., and Ginder, G. D. (1994) *Am. J. Pediatr. Hematol. Oncol. 16*, 67−71.
15. Collins, A. F., Pearson, H. A., Giardina, P., McDonagh, K. T., Brusilow, S. W., and Dovver, G. J. (1995) *Blood 85*, 43−49.
16. Faller, D. V., and Perrine, S. P. (1995) *Curr. Opin. Hematol. 2*, 109−117.
17. Pace, B. S., Li, Q., and Stomatoyannopoulos, G. (1996) *Blood 88*, 1079−1083.
18. Maier-Redelsperger, M., Labie, D., and Elion, J. (1999) *Curr. Opin. Hemat. 6*, 115−120.
19. Loukopoulos, D., Voskaridou, E., Kalotychou, V., Schina, M., Loutradi, A., and Theodoropoulos, I. (2000) *Blood Cells, Mol. Dis. 26*, 453−466.
20. Dickerson, R. E., and Geis, I. (1983) *Hemoglobin: Structure, Function, Evolution, and Pathology*, Benjamin/Cummings, Menlo Park, CA.
21. Coletta, M., Angeletti, M., DeSanctis, G., Cerroni, L., Giardina, B., Amiconi, G., and Ascenzi, P. (1996) *Eur. J. Biochem. 235*, 49−53.
22. Brittain, T. (2000) *J. Inorg. Biochem. 81*, 99−103.
23. Russell, J. E., and Liebhaber, S. A. (1998) *Blood 92*, 3057−3063.
24. Liebhaber, S. A., Wang, Z., Cash, F. E., Monks, B., and Russell, J. E. (1996) *Mol. Cell Biol. 16*, 2637−2646.
25. Morales, J., Russell, J. E., and Liebhaber, S. A. (1997) *J. Biol. Chem. 272*, 607−6613.
26. He, Z., Lian, L., Asakura, T., and Russell, J. E. (2000) *Br. J. Haematol. 109*, 882−890.
27. Zheng, T., Brittain, T., Watmough, N. J., and Weber, R. E. (1999) *Biochem. J. 343*, 681−685.
28. Zheng, T., Zhu, Q., and Brittain, T. (1999) *IUBMB Life 48*, 435−437.
29. Cudney, R., Patel, S., Weisgraber, K., Newhouse, Y., and McPherson, A. (1994) *Acta Crystallogr. D50*, 414−423.
30. Matthews, B. W. (1968) *J. Mol. Biol. 33*, 491−497.
31. Otwinowski, Z., and Minor, W. (1997) *Methods Enzymol. 276*, 307−326.
32. Silva, M. M., Rogers, P. H., and Arnone, A. (1992) *J. Biol. Chem. 267*, 17248−17256.
33. Brünger, A. T., Adams, P. D., Clore, G. M., DeLano, W. L., Gros, P., Grosse-Kunstleve, R. W., Jiang, J.-S., Kuszewski, J., Nilges, M., Pannu, N. S., Read, R. J., Rice, L. M., Simonson, T., and Warren, G. L. (1999) *Acta Crystallogr. D54*, 905−921.
34. Brünger, A. T. (1992) *Nature 355*, 472−475.
35. Jones, T. A., Zou, J. Y., Cowan, S. W., and Kjeldgaard, M. (1991) *Acta Crystallogr. A47*, 110−119.
36. Popp, R. A. (1973) *Biochim. Biophys. Acta 303*, 52−60.
37. Collaborative Computational Project, Number 4. (1994) *Acta Crystallogr. D50*, 760−763.
38. Laskowski, R. A., MacArthur, M. W., Moss, D. S., and Thornton, J. M. (1993) *J. Appl. Crystallogr. 26*, 283−291.
39. He, Z., and Russell, J. E. (2001) *Blood 97*, 1099−1105.
40. Mazzarella, L., D'Avino, R., di Prisco, G., Savino, C., Vitagliano, L., Moody, P. C. E., and Zagari, A. (1999) *J. Mol. Biol. 287*, 897−906.
41. Sutherland-Smith, A. J., Baker, H. M., Hofmann, O. M., Brittain, T., and Baker, E. N. (1998) *J. Mol. Biol. 280*, 475−484.
42. Heaslet, H. A., and Royer, Jr., W. E. (1999) *Structure 7*, 517−526.
43. Shaanan, B. (1983) *J. Mol. Biol. 171*, 31−59.
44. Kidd, R. D., Baker, H. M., Mathews, A. J., Brittain, T., and Baker, E. N. (2001) *Protein Sci. 10*, 1739−1749.
45. Frier, J. A., and Perutz, M. F. (1977) *J. Mol. Biol. 112*, 97−112.
46. Robson, N., and Brittain, T. (1996) *J. Inorg. Biochem. 64*, 137−147.
47. Roy, R. P., Nacharaju, P., Magel, R. L., and Acharya, A. S. (1995) *J. Protein Chem. 14*, 81−88.
48. Riggs, A., and Herner, A. E. (1962) *Proc. Natl. Acad. Sci. U.S.A. 48*, 1664−1670.
49. Abraham, D. J., Kellog, G. E., Holt, J. M., and Ackers, G. K. (1997) *J. Mol. Biol. 272*, 613−632.
50. Clegg, J. B., and Gagnon, J. (1981) *Proc. Natl. Acad. Sci. U.S.A. 78*, 6076−6080.
51. Stegink, L. D., Meyer, P. D., and Brunnel, M. C. (1971) *J. Biol. Chem. 246*, 3001−3007.
52. Kraulis, P. J. (1991) *J. Appl. Crystallogr. 24*, 946−950.
53. Merritt, E. A., and Murphy, M. E. P. (1994) *Acta Crystallogr. D50*, 869−873.
54. Esnouf, R. M. (1997) *J. Mol. Graphics Modell. 15*, 132−134.

BI011329F